



## Three-dimensional influence coefficient method for cohesive crack simulations

James H. Hanson<sup>a,\*</sup>, Tulio N. Bittencourt<sup>b</sup>, Anthony R. Ingraffea<sup>c</sup>

<sup>a</sup> *Rose-Hulman Institute of Technology, Department of Civil Engineering, Terre Haute, IN 47803, USA*

<sup>b</sup> *Departamento de Engenharia de Estruturas e Fundações, Escola Politécnica da Universidade de São Paulo, 05508-900 São Paulo, SP, Brazil*

<sup>c</sup> *Civil and Environmental Engineering, Cornell University, 220 Hollister Hall, Ithaca, NY 14853, USA*

Received 1 July 2002; received in revised form 25 December 2003; accepted 29 December 2003

### Abstract

The influence coefficient method, which has advantages for conducting inverse analysis and sensitivity studies, is extended to simulate cohesive cracking in three-dimensional bodies when the crack path is known in advance. The method is combined with a focal point model to allow simulation of unload–reload cycles as well. This paper summarizes the theory behind the influence coefficient method and outlines how the method can be implemented in a numerical simulation program. The scaling factor technique is presented in order to use a single set of influence coefficients to simulate the response of identical bodies made of materials with different moduli of elasticity.

© 2004 Elsevier Ltd. All rights reserved.

*Keywords:* Three-dimensional numerical simulation; Non-linear fracture mechanics; Cohesive crack modeling; Unload–reload cycle; Influence coefficients

### 1. Introduction

Cohesive crack simulations are becoming increasingly popular among researchers for numerically simulating crack propagation under non-linear fracture mechanics conditions [1–9]. One application of these simulations is in determining the cohesive zone constitutive relationship for a material. The process by which this is done is called inverse analysis data reduction [10–13]. Inverse analysis requires many numerical simulations of a laboratory test specimen in order to determine the cohesive zone property values.

The cohesive zone constitutive relationship can be incorporated into numerical simulations via interface finite elements [14–16]. However, the use of interface elements is computationally most efficient when the response of the simulated body is only calculated a few times. When the response must be calculated many times, such as for inverse analysis or sensitivity studies, the influence coefficient method can be computationally more efficient.

\* Corresponding author. Fax: +1-812-877-8440.

E-mail address: [james.hanson@rose-hulman.edu](mailto:james.hanson@rose-hulman.edu) (J.H. Hanson).

This paper details how the influence coefficient method can be implemented for numerical simulation of three-dimensional bodies with a cohesive crack. An advantage of implementing the method in three dimensions is that the crack front is not constrained to be straight and the crack path need not be straight. A limitation of the method is that the crack path must be known a priori. When the method is used with a cohesive zone constitutive relationship for unloading, the method can also simulate the response of a cracked body when unloaded. Issues of mesh dependence and computational effort are discussed.

To enhance the computational efficiency of the influence coefficient method, the scaling factor technique has been developed. This technique allows the use of one set of influence coefficients, generated for a body with a particular modulus of elasticity, to simulate the response of an identical body with a different modulus of elasticity. Therefore, a single set of influence coefficients can be used repeatedly when applying inverse analysis to results from the same test specimen size and geometry but different materials.

## 2. Cohesive crack simulations

### 2.1. Cohesive zone constitutive relationship

The defining characteristic of a cohesive crack simulation is that all of the crack region non-linear behavior is represented by the constitutive relationship between crack opening displacement, COD, and cohesive traction,  $\sigma$ , along the crack path. This model for non-linear crack propagation was first proposed by Dugdale [17] and Barrenblatt [18]. Since then, researchers have used cohesive zone relationships of different shapes to simulate crack propagation in materials such as metals, polymers, and concrete [1–9].

The cohesive zone constitutive relationship describes the relationship between cohesive traction and COD after the local tensile capacity of the material has been reached (Fig. 1). Although the shape of the relationship might differ for various materials, all cohesive zone relationships share three common parameters: tensile capacity,  $f_t$ , characteristic crack opening displacement,  $w_c$ , and area under the graph,  $G_{Ic}^{coh}$ , critical energy release rate. For COD's greater than  $w_c$ , the relationship dictates that no cohesive traction is transferred across the crack.

The cohesive crack model for crack propagation asserts that the COD remains zero until  $f_t$  is achieved. This corresponds to an infinite slope for the initial portion of the relationship as the traction between the potential crack faces increases to  $f_t$ . To avoid the numerical problems of infinite slope, the initial slope can be approximated with a large, finite value (Fig. 2). The initial slope is called the initial stiffness,  $k_c$ , and should be set as large as possible so that the COD at the tensile strength,  $w_{f_t}$ , is close to zero. Although  $k_c$  must be specified to implement the cohesive crack model numerically, the initial stiffness is not considered a characteristic of the cohesive zone constitutive relationship. The authors have found that a  $k_c$  on the order

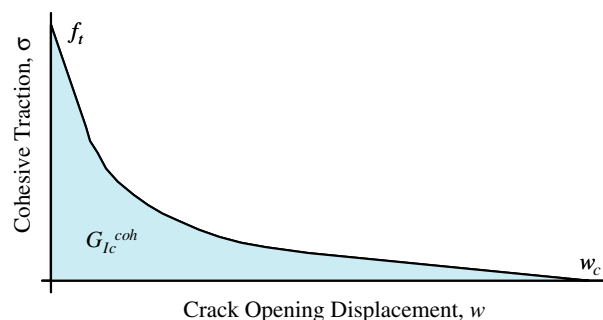


Fig. 1. Cohesive zone constitutive relationship.

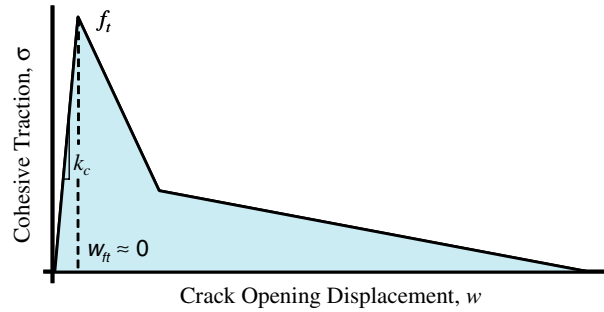


Fig. 2. Numerical implementation of the cohesive zone constitutive relationship.

of the modulus of elasticity,  $E$ , divided by the characteristic crack opening displacement,  $w_c$ , results in negligible CODs before the tensile strength limit is reached without causing any numerical instabilities. Smaller values of  $k_c$  might produce comparable results but have not been explored.

2.2. Inverse analysis and sensitivity studies

One application of cohesive crack simulations is inverse analysis. Inverse analysis is a data reduction method for obtaining the cohesive zone constitutive relationship values from load versus displacement data from laboratory tests. Several researchers have used this data reduction method [10–13].

The basic components of inverse analysis are illustrated in Fig. 3. Cohesive crack simulations are used to generate a simulated specimen response similar to the measured response. The input cohesive zone property values for the simulations are systematically changed until the simulated response acceptably matches the measured response. When the responses agree, the input property values are taken to be reasonable estimates of the cohesive constitutive properties for the laboratory specimen.

This data reduction method requires a significant number of cohesive crack simulations in order to determine the cohesive zone property values. Therefore, the inverse analysis data reduction method would

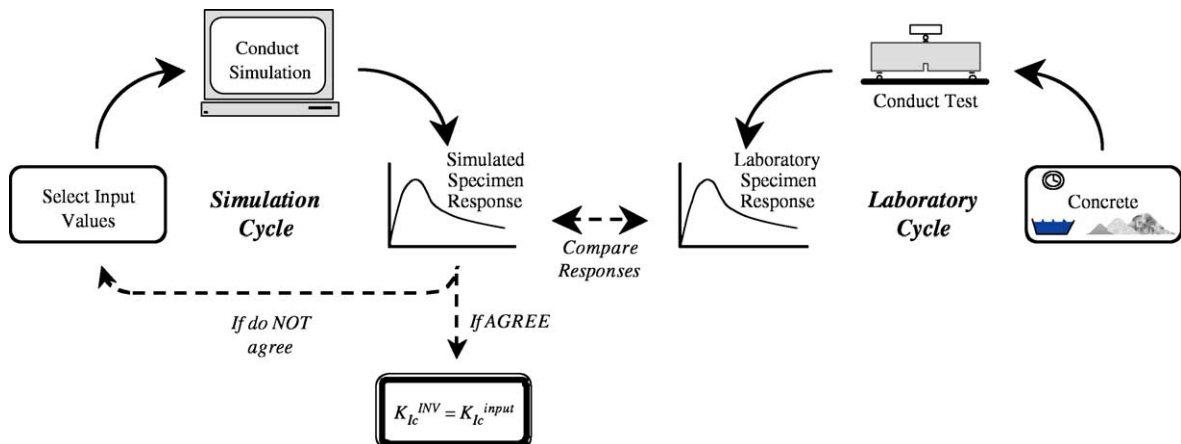


Fig. 3. Schematic of the inverse analysis data reduction method.

benefit from a computationally efficient algorithm for solving many cohesive crack simulations for a specific test specimen size and geometry.

For some structures, the behavior of the structure is very sensitive to the cohesive zone constitutive relationship. For other structures, the behavior is relatively insensitive to the relationship. Studies are often performed to determine the magnitude of this sensitivity. Such studies might require many analyses of the same structure using different cohesive zone constitutive relationships. Therefore, sensitivity studies would also benefit from a computationally efficient algorithm for solving many cohesive crack simulations for a specific structure.

### 2.3. Interface elements

Interface elements are a commonly used tool for cohesive crack simulations [14–16]. The cohesive zone constitutive relationship is included in the formulation of the interface element stiffness coefficients while the other elements remain linear elastic. The numerical simulations are often performed based on the direct stiffness method. The governing expression of the direct stiffness method is given in Eq. (1) where  $F$  is the vector of applied force at every unrestrained degree of freedom, DOF,  $\Delta$  is the vector of resulting displacement at each unrestrained DOF, and  $K(\Delta)$  is the matrix of finite element stiffness coefficients. Because of the constitutive relationship of the interface elements, some of the stiffness coefficients depend on the displacements; therefore, Eq. (1) is a non-linear system of equations. To simulate the response of a body to an applied load or displacement requires an iterative solution of Eq. (1), Fig. 4. Each point on a simulated load versus displacement curve is one solution of Eq. (1). If many points must be calculated for a specific body, the interface element approach can be computationally expensive.

$$F = K(\Delta)\Delta \quad (1)$$

### 2.4. Influence coefficients

Petersson [19] proposed a method for cohesive crack simulation that consists of superimposing the effects of applied forces and the effects of cohesive tractions on a linear elastic body. Therefore, cohesive crack simulation can be performed using a matrix of influence coefficients generated from linear elastic simulations. The method was called the “influence method” [20] and was enhanced by several authors [20–22]. Bittencourt and coworkers [9,22–24] implemented the method for simulation of three-dimensional bodies

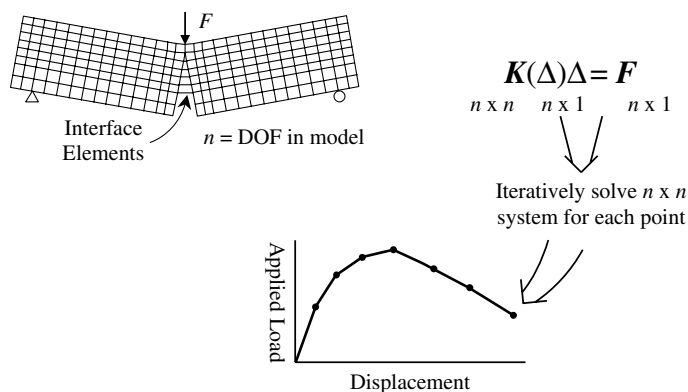


Fig. 4. Schematic of generating a simulated response graph from cohesive crack simulations using interface elements.

and added the capability of simulating unloading behavior. He developed these capabilities in a program called CohFRANC3D.<sup>1</sup> The implementation in CohFRANC3D has been further enhanced and is described in detail in the next section as an example of how to implement the influence coefficient method.

The influence coefficient method for cohesive crack simulations is formulated as a flexibility method. The governing expression is in the form of Eq. (2) where  $\mathbf{\Delta}$  is as defined in Eq. (1),  $\mathbf{F}(\mathbf{\Delta})$  is the vector of cohesive forces on the crack face and only non-zero applied forces, and  $\mathbf{B}$  is the matrix of flexibility influence coefficients. As shown in Fig. 1, the cohesive forces depend on the displacements.

$$\mathbf{\Delta} = \mathbf{BF}(\mathbf{\Delta}) \quad (2)$$

The influence coefficient method asserts that the CODs of the crack face nodes can be expressed as the sum of CODs due to applied surface tractions and cohesive tractions on the crack face. Only the coefficients related to the COD degrees of freedom are needed to calculate the CODs and associated cohesive tractions. This system of equations is much smaller than the system that describes the displacements everywhere in the simulated body (Fig. 5). The cohesive zone constitutive relationship is contained in this smaller system of equations, which must be solved iteratively. Displacements everywhere in the body are calculated by substituting the calculated surface traction and cohesive tractions back into Eq. (2) in  $\mathbf{F}(\mathbf{\Delta})$ .

Each influence coefficient is the COD at a specific crack face node due to a unit traction, not force, applied at a specific crack face node or on a user specified, non-crack surface (i.e., the surface of a test specimen that is loaded in the laboratory). The traction on the non-crack surface is uniform across the entire surface. When the traction is applied to crack face nodes, the traction is unity at the specified node and varies linearly to zero at the adjacent nodes. If the boundary element method, BEM, is used to generate the influence coefficients, the applied traction is as shown in Fig. 6. If the finite element method, FEM, is used, the applied traction must be converted to work-equivalent nodal loads (Fig. 7). Currently, the CohFRANC3D program uses the BEM to generate the influence coefficients.

The influence coefficient method requires significant computational effort to generate the influence coefficients,  $\mathbf{B}$ . However, once the coefficients have been obtained, the simulated response can be calculated with much less computational effort. Therefore, the influence coefficient method might be more efficient than the non-linear interface element method when generating many cohesive crack solutions for a particular body. An example of computational effort required using influence coefficients is presented later.

When using influence coefficients for cohesive crack simulations, the user specifies how far the crack front has advanced. The load applied to the simulated body to advance the cohesive crack to that front limit is determined in the solution process. Therefore, response in the snap-back regime can be simulated.

### 3. Implementation of the influence coefficient method

#### 3.1. Governing equations

The underlying assumption of the influence coefficient method is that the COD at any node on the crack face can be expressed as a superposition of linear elastic responses to cohesive tractions on any of the crack face nodes and tractions applied on user specified non-crack surfaces. This relationship can be expressed as Eq. (3). In this equation,  $\mathbf{w}$  is the vector of CODs. The matrix  $\mathbf{D}$  consists of compliance influence coefficients,  $D_{ij}$ . Each term is the COD response at the  $i$ th crack face node due to a unit cohesive traction applied at the  $j$ th crack face node. Therefore,  $\mathbf{D}$  is a subset of  $\mathbf{B}$  in Eq. (2). The vector  $\boldsymbol{\sigma}(\mathbf{w})$  consists of tractions on the crack face nodes,  $\sigma_j(w_j)$ . Each term is the traction applied to the  $j$ th crack face node. If the COD at the

<sup>1</sup> CohFRANC3D is a program developed and enhanced by members of the Cornell Fracture Group [10,21,25,26].

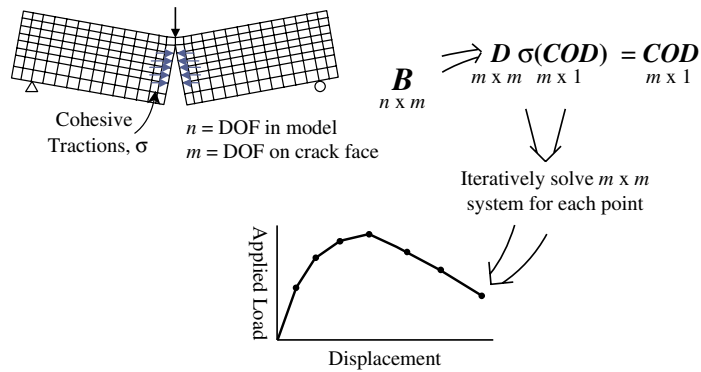


Fig. 5. Schematic of generating a simulated response graph from cohesive crack simulations using influence coefficients.

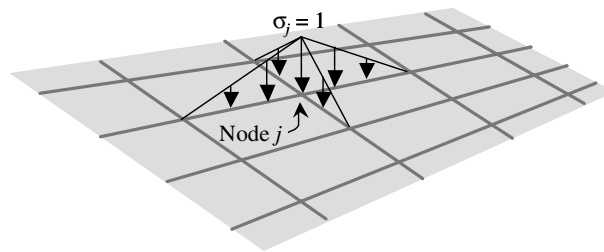


Fig. 6. Application of a unit traction to a boundary element model to generate influence coefficients.

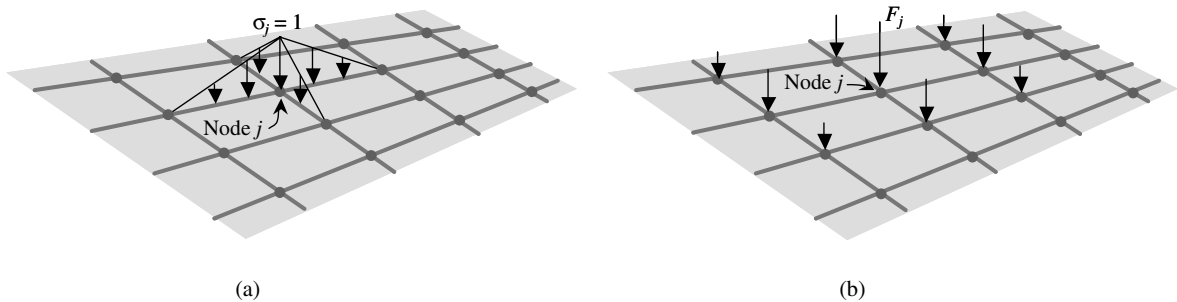


Fig. 7. Application of a unit traction to a finite element model to generate influence coefficients: (a) schematic of application of the unit traction, and (b) work-equivalent nodal loads.

$j$ th crack face node is non-zero,  $w_j > 0$ , the traction value depends upon the value of the COD at that node. The relationship between traction and COD is given by the cohesive zone constitutive relationship. The vector  $\mathbf{d}$  consists of compliance influence coefficients,  $d_i$ . Each term is the COD response at the  $i$ th crack face node due to a unit traction applied to all surfaces designated by the user as being externally loaded. Therefore,  $\mathbf{d}$  is also a subset of  $\mathbf{B}$  in Eq. (2). The scalar  $F$  is the actual traction magnitude applied to those designated surfaces.

$$\mathbf{w} = \mathbf{D}\sigma(\mathbf{w}) + F\mathbf{d} \tag{3}$$

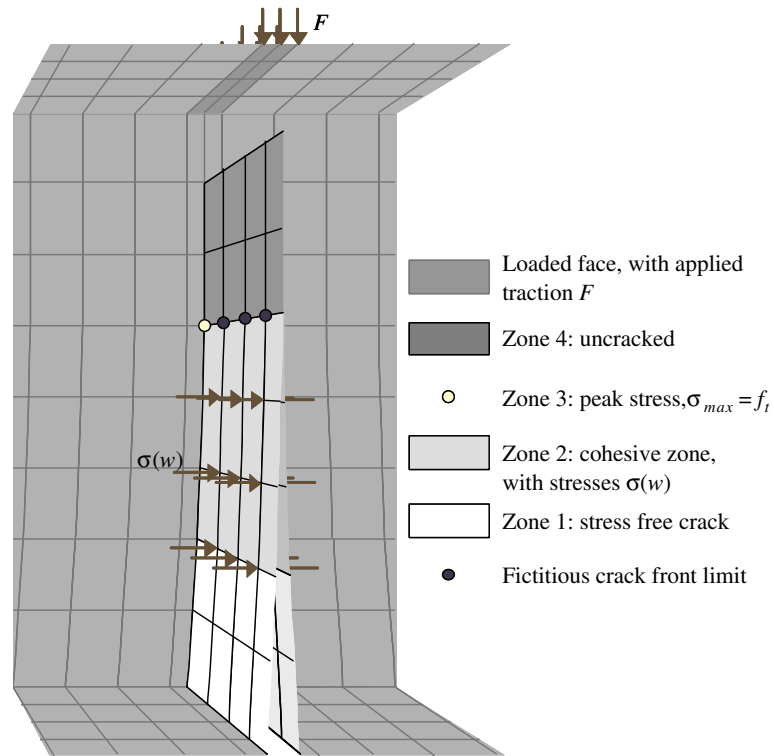


Fig. 8. Zones of the crack face of a simulation model.

The crack face node traction,  $\sigma_j$ , depends on the crack opening displacement,  $w_j$ , at that node. To describe the rules for calculating the traction, the authors have designated four zones denoted by the superscripts I–IV (Fig. 8). Zone I consists of all nodes that are free of cohesive traction. This zone is also called the “true crack” zone. For these nodes,  $w_j \geq w_c$ , where  $w_c$  is the characteristic crack opening displacement, and  $\sigma_j = 0$ . Zone II consists of all nodes in the “cohesive crack” zone. For these nodes,  $w_c \geq w_j > 0$  and the cohesive traction is governed by the cohesive zone constitutive relationship,  $\sigma_j = \sigma_j^{\text{II}}(w_j)$ . Zone IV consists of all nodes in the “uncracked” zone. For these nodes,  $w_j = 0$  and  $\sigma_j^{\text{IV}} < f_t$ . There is no compressive traction limit on  $\sigma_j^{\text{IV}}$ .

In a continuum, there would be a boundary between material designated Zone II and material designated Zone IV. That boundary would be the location where the tensile traction,  $\sigma$ , just reaches the tensile strength of the cohesive zone constitutive relationship,  $f_t$ . That boundary is called the fictitious crack front. The term “fictitious” is used to distinguish it from the front of the “true crack” zone. In a discretized three-dimensional body, the fictitious crack front might run along nodes or between nodes. To find a unique solution to Eq. (3), at least one point on the fictitious crack front must be identified. That point is a node selected by the user and is designated Zone III. Therefore, Zone III consists of just one node, the node selected to experience tensile traction equal to  $f_t$ .

To limit advance of the fictitious crack front when solving Eq. (3), a fictitious front limit can be identified. The fictitious front limit is a user-defined set of nodes that crosses the entire crack face. One of the nodes on the fictitious front limit is assigned to Zone III. If the solution of Eq. (3) indicates that a node on the fictitious front limit reached a tensile traction greater than  $f_t$ , that node is designated as the Zone III

node and Eq. (3) is evaluated again. Therefore, the fictitious front is ensured to not pass the fictitious front limit.

Each time the user advances the fictitious front limit, Eq. (3) must be solved again, thus producing a new simulated response. If the solution of Eq. (3) indicates that some Zone II nodes near the fictitious front limit have not reached the tensile strength,  $f_t$ , those nodes enter Zone IV. Eq. (3) can be expanded to produce Eq. (4) where the superscripts refer to the four zones.

$$\begin{Bmatrix} w^I \\ w^{II} \\ w^{III} \\ w^{IV} \end{Bmatrix} = \begin{bmatrix} D^{I,I} & D^{I,II} & D^{I,III} & D^{I,IV} \\ D^{II,I} & D^{II,II} & D^{II,III} & D^{II,IV} \\ D^{III,I} & D^{III,II} & D^{III,III} & D^{III,IV} \\ D^{IV,I} & D^{IV,II} & D^{IV,III} & D^{IV,IV} \end{bmatrix} \begin{Bmatrix} \sigma^I \\ \sigma^{II} \\ \sigma^{III} \\ \sigma^{IV} \end{Bmatrix} + F \begin{Bmatrix} d^I \\ d^{II} \\ d^{III} \\ d^{IV} \end{Bmatrix} \quad (4)$$

Each zone has a prescribed boundary condition. These boundary conditions are summarized in Eqs. (5a)–(5e).

$$\sigma^I = \mathbf{0} \quad (5a)$$

$$\sigma^{II} = \sigma^{II}(w^{II}) \quad (5b)$$

$$\sigma^{III} = f_t \quad (5c)$$

$$w^{III} = 0 \quad (5d)$$

$$w^{IV} = \mathbf{0} \quad (5e)$$

Inserting the boundary conditions of Eq. (5) into Eq. (4) and rearranging terms leads to Eq. (6) where  $\mathbf{I}$  is the identity matrix.

$$\begin{bmatrix} \mathbf{I} & \mathbf{0} & -D^{I,IV} & -d^I \\ \mathbf{0} & \mathbf{I} & -D^{II,IV} & -d^{II} \\ \mathbf{0} & \mathbf{0} & -D^{III,IV} & -d^{III} \\ \mathbf{0} & \mathbf{0} & -D^{IV,IV} & -d^{IV} \end{bmatrix} \begin{Bmatrix} w^I \\ w^{II} \\ \sigma^{IV} \\ F \end{Bmatrix} = \begin{Bmatrix} D^{I,II}\sigma^{II}(w^{II}) + f_t D^{I,III} \\ D^{II,II}\sigma^{II}(w^{II}) + f_t D^{II,III} \\ D^{III,II}\sigma^{II}(w^{II}) + f_t D^{III,III} \\ D^{IV,II}\sigma^{II}(w^{II}) + f_t D^{IV,III} \end{Bmatrix} \quad (6)$$

Let  $\mathbf{C}$  represent the matrix on the left side of Eq. (6),  $\mathbf{u}$  represent the unknowns, and  $\mathbf{g}(\mathbf{u})$  represent the right side of Eq. (6). This substitution results in the more compact equation (7). Eq. (7) is the governing expression describing all cohesive crack solutions using influence coefficients. The vector  $\mathbf{g}$  is a function of  $\mathbf{u}$  because the magnitude of the cohesive traction at a node in Zone II,  $\sigma_j^{II}$ , depends upon the COD at that node,  $w_j^{II}$ .

$$\mathbf{C}\mathbf{u} = \mathbf{g}(\mathbf{u}) \quad (7)$$

### 3.2. Solving the governing equations

Because  $\mathbf{g}$  in the governing expression depends upon the unknowns,  $\mathbf{u}$ , Eq. (7) is a system of non-linear equations. The algorithm described in Fig. 9 can be used to solve these equations. Numerical schemes such as Newton–Raphson or Modified Newton–Raphson can be used to calculate the incremental change of the solution.

Define  $\mathbf{e}(\mathbf{u})$  as the vector of residuals as shown in Eq. (8). Then the  $n$ th increment toward the solution,  $\Delta\mathbf{u}_n$ , is calculated by Eq. (9) for the Newton–Raphson scheme or Eq. (10) for the Modified Newton–Raphson scheme. To quantify the residual error,  $\mathbf{e}(\mathbf{u})$ , calculate the norm of the residual error vector. One possibility is the Euclidean norm given by Eq. (11).

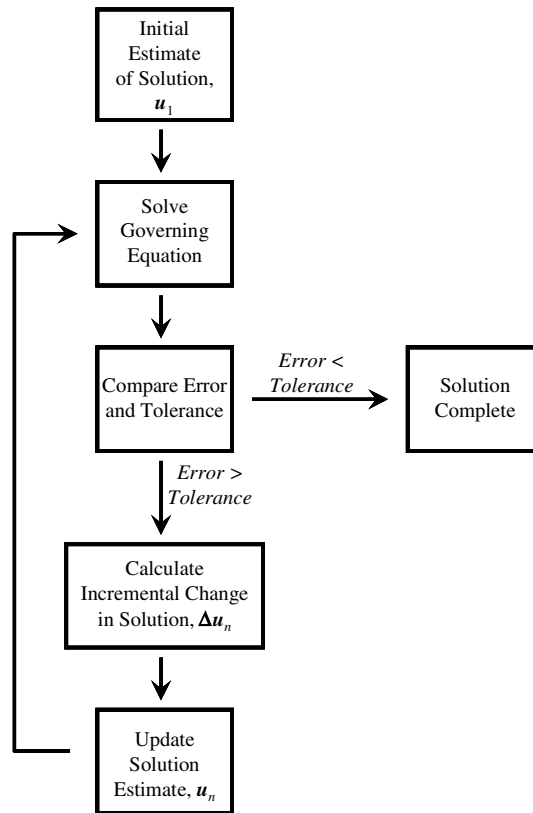


Fig. 9. Solution algorithm used by CohFRANC3D to solve the governing equations.

$$e(\mathbf{u}) = \mathbf{C}\mathbf{u} - \mathbf{g}(\mathbf{u}) \tag{8}$$

$$-\left[ \mathbf{C} - \frac{\partial \mathbf{g}(\mathbf{u})}{\partial \mathbf{u}} \Big|_{\mathbf{u}_{n-1}} \right]^{-1} e(\mathbf{u}_{n-1}) = \Delta \mathbf{u}_n \tag{9}$$

$$-\mathbf{C}^{-1} e(\mathbf{u}_{n-1}) = \Delta \mathbf{u}_n \tag{10}$$

$$\|e(\mathbf{u})\|_2 = \sqrt{\sum_i [e_i(\mathbf{u})]^2} \tag{11}$$

Note that the term in brackets in Eq. (9) must be recalculated and inverted with each iteration. Because the Modified Newton–Raphson scheme uses only the term  $\mathbf{C}$  in the brackets, the inverted value of  $\mathbf{C}$  in Eq. (10) does not need to be recalculate with each iteration. However, the Modified Newton–Raphson scheme will typically require more iterations to converge compared to the Newton–Raphson scheme.

Neither the Newton–Raphson nor the Modified Newton–Raphson scheme is guaranteed to converge. For cases where the solution to the system of equations does not converge, multiplying  $\Delta \mathbf{u}_n$  in Eq. (9) or (10) by a relaxation factor before updating the solution,  $\mathbf{u}_n$ , can help the system converge. The relaxation factor is a positive number less than one. The authors have successfully used relaxation factors from 0.8 to 0.003. Using a smaller relaxation factor increases the likelihood of convergence but requires more iterations.

3.3. Generating unloading response

Residual deformation has been observed when fracture test specimens of some materials are unloaded [27–30]. This residual crack opening can be predicted using influence coefficients. Once the governing expression, Eq. (7), has been solved for a non-zero applied traction, the cohesive zone constitutive relationship used with Zone II nodes can be replaced with a relationship developed for unloading. One such relationship, the focal point model, was developed for concrete by Yankelevsky and Reinhardt [31]. This new expression can be solved for the crack face tractions and crack opening displacements of the simulated specimen as it *unloads*.

The focal point model is a phenomenological model that describes the traction versus displacement response of concrete in uniaxial tension as it is unloaded and reloaded in the tension softening regime. The general shape of an unload–reload curve according to the focal point model is shown in Fig. 10. The model uses fixed points, called focal points, to determine the slope of the various parts of the unload–reload curve. By observing that they could use focal points, Yankelevsky and Reinhardt were able to write general expressions for the coordinates of the unload–reload curve based only upon the tensile strength of the concrete,  $f_t$ , and the point at which unloading began,  $w^A$  and  $\sigma^A$ . The expressions do not depend upon  $w_c$  or the shape of the cohesive zone relationship. It is important to note that some expressions for the coordinates presented by Yankelevsky and Reinhardt (specifically Eqs. (13), (17) and (19)) contain errors. The correct versions of Yankelevsky and Reinhardt [31] Eqs. (13), (17) and (19) are presented here in Eqs. (12)–(14), respectively. Eqs. (12)–(14) use the same notation as in [31].

$$C_3 = \frac{3(f_t \cdot S_A + \sigma_A \cdot S_2)}{3f_t + \sigma_A} \tag{12}$$

$$D_2 = -\frac{\sigma_6}{S_B + \frac{S_2 \cdot \sigma_6}{f_t}} \tag{13}$$

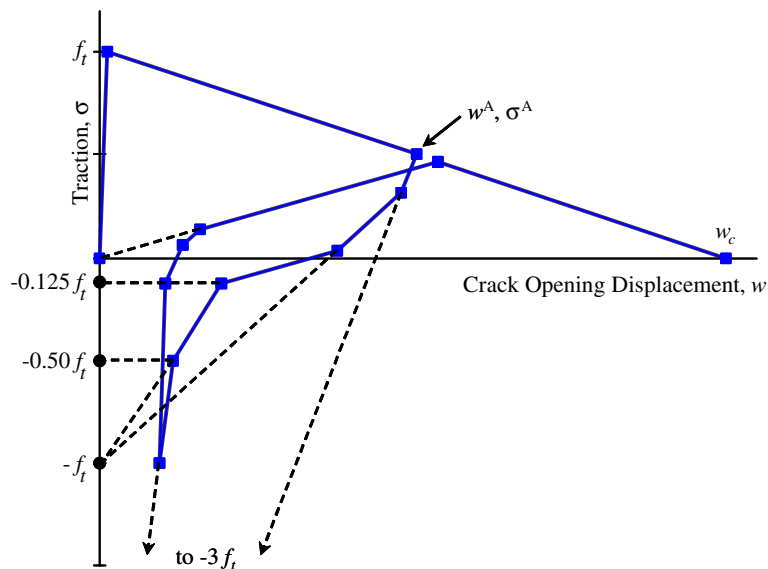


Fig. 10. Schematic of an unload–reload cycle according to the focal point model for concrete.

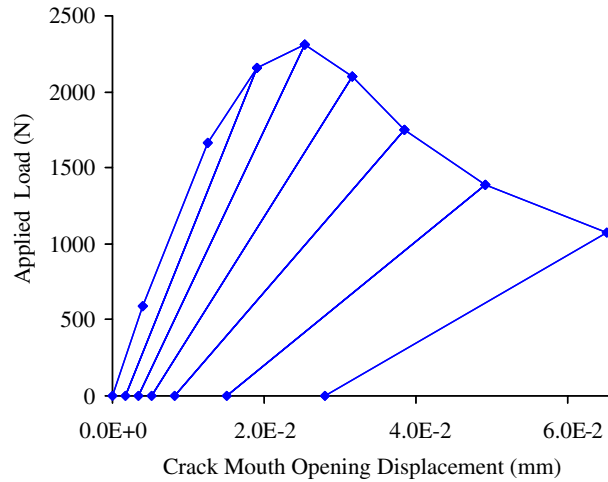


Fig. 11. Simulated load–deflection response of a single edge specimen loaded in bending.

$$\sigma_6 = \frac{0.075 f_t \cdot S_B}{-0.075 \cdot S_2 + 0.5 \cdot S_A - S_B} \tag{14}$$

To simulate unloading, the prescribed boundary conditions in Eqs. (5a)–(5e) remain the same except that (5c) no longer applies and  $F$  must be prescribed. With these changes, Eq. (6) becomes Eq. (15). For the case of unloading, the focal point model rather than the cohesive zone constitutive relationship is used to describe the traction versus COD behavior of each of the Zone II nodes. Before beginning the solution of Eq. (15), the current vector of Zone II CODs,  $w^{II}$ , and tractions,  $\sigma^{II}$ , defines the point  $A$ ,  $(w_j^A, \sigma_j^A)$ , from Fig. 10 for each of the Zone II nodes. This results in a different unload path for each of the Zone II nodes. The unload path becomes the relationship between  $\sigma_j^{II}$  and  $w_j^{II}$  used in Eq. (15). By setting  $F$  in Eq. (15) to a portion of the applied traction calculated from Eq. (9), the system of equations can be solved to find any point on the unloading curve for the simulated specimen. The same solution schemes described to solve Eq. (6) can be used to solve Eq. (15).

$$\begin{bmatrix} \mathbf{I} & \mathbf{0} & -\mathbf{D}^{I,IV} & -\mathbf{D}^{I,III} \\ \mathbf{0} & \mathbf{I} & -\mathbf{D}^{II,IV} & -\mathbf{D}^{II,III} \\ \mathbf{0} & \mathbf{0} & -\mathbf{D}^{III,IV} & -\mathbf{D}^{III,III} \\ \mathbf{0} & \mathbf{0} & -\mathbf{D}^{IV,IV} & -\mathbf{D}^{IV,III} \end{bmatrix} \begin{Bmatrix} w^I \\ w^{II} \\ \sigma^{IV} \\ \sigma^{III} \end{Bmatrix} = \begin{Bmatrix} \mathbf{D}^{I,II} \sigma^{II}(w^{II}) + F d^I \\ \mathbf{D}^{II,II} \sigma^{II}(w^{II}) + F d^{II} \\ \mathbf{D}^{III,II} \sigma^{II}(w^{II}) + F d^{III} \\ \mathbf{D}^{IV,II} \sigma^{II}(w^{II}) + F d^{IV} \end{Bmatrix} \tag{15}$$

By solving Eqs. (6) and (15) for different fictitious front limits, the response of a body to loading and unloading can be predicted. Fig. 11 is an example of a load versus crack mouth opening displacement graph for a simulated single edge specimen loaded in bending, SE(B). The simulation geometry is shown in Fig. 12, and the cohesive zone constitutive relationship values are shown in Fig. 13.

#### 4. Computational issues

##### 4.1. Mesh dependence

The accuracy of the solution of Eqs. (6) and (15) is dependent upon the accuracy of the matrices of influence coefficients  $\mathbf{D}$  and  $\mathbf{d}$ . Each influence coefficient is calculated as the response of a deeply cracked,

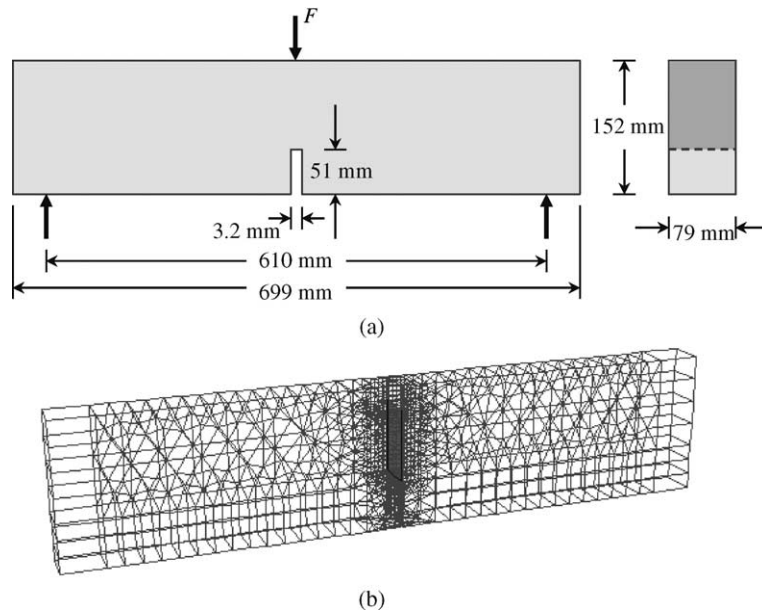


Fig. 12. Simulated single edge beam loaded in bending: (a) geometry, and (b) boundary element mesh.

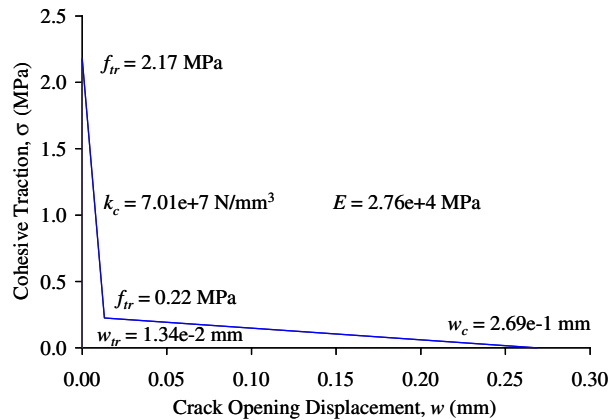


Fig. 13. Cohesive zone constitutive relationship used with in the example simulation of an SE(B).

linear elastic body to a unit traction on either a crack face node or a unit traction on a non-crack surface specified by the user. If the linear elastic simulation is not accurate, the cohesive crack simulation cannot be accurate. Inaccuracies in the simulated linear elastic response typically occur because of the performance of the mesh.

The accuracy of the influence coefficients can be evaluated by comparing them with either an analytical solution or a converged linear elastic finite element solution. If the errors in the influence coefficients are unacceptably large, the mesh should be changed. The region with the highest gradient of deformation is around the crack front in the linear elastic model. Refining the mesh in that region might improve the accuracy of the influence coefficients.

#### 4.2. Computational effort

A goal of any numerical simulation is to obtain an acceptable result with reasonable effort. For the cohesive crack simulations using influence coefficients, most of the computational effort is spent generating the influence coefficients,  $\mathbf{B}$  in Eq. (2). The total amount of effort required depends upon the total number of degrees of freedom in the simulation and the number of crack face nodes. To calculate a column of coefficients in  $\mathbf{B}$ , CohFRANC3D uses boundary elements and solves an expression similar to Eq. (1) for a unit traction applied normal to the crack face at a single crack face node. Therefore, the expression must be solved as many times as there are crack face nodes. Memory limitations of the computer generating the entire matrix of influence coefficients,  $\mathbf{B}$ , might restrict the number of DOF of the simulation including crack face nodes. Because the expression similar to Eq. (1) must be solved once for each crack face node, time limitations might restrict the number of crack face nodes that the simulation can have. Both time and memory constraints should be considered when selecting the optimum mesh for the simulation.

In generating the influence coefficients, the mesh does not change, only the location of the unit traction changes. Such a system of equations is said to have “multiple right hand sides”. Efficient numerical methods such as Cholesky or LU decomposition [32] can be used to generate the many columns of coefficients in  $\mathbf{B}$ . By using one of these methods, the time required to generate the second through last columns in  $\mathbf{B}$  is small compared to the time required to solve Eq. (1) once to generate the first column.

As an example of computing resources required to solve a large problem, consider the simulation model in Fig. 12. The influence coefficients for this model required 21 min to generate using 24 processors from an IBM SP supercomputer.<sup>2</sup> The simulation had 5269 DOF,  $n$ , and 108 crack face nodes,  $m$ . If the influence coefficients had been generated on a single processor, the system of equations would have required 222 Mbytes of memory to store. The output file with the entire  $\mathbf{B}$  matrix required 66.9 Mbytes of disk space.

Fortunately, the entire file of influence coefficients is not required to solve the governing system, Eq. (6) or (15). Those equations only require the coefficients of the applied traction and crack face tractions on the crack face opening DOF. The complete set of influence coefficients quantifies the effects of those tractions on every DOF in the simulation. In CohFRANC3D, the influence coefficients needed to solve Eqs. (6) and (15),  $\mathbf{D}$  and  $\mathbf{d}$ , are extracted and put into a new file. For the example above, this file required only 285 kbytes to store. The time required to solve Eq. (6) or (15) for the example above ranged from 1 to 30 s on a single DEC Alpha workstation.<sup>3</sup> The computational effort to solve Eq. (6) or (15) is much smaller than the effort to generate the entire coefficient matrix,  $\mathbf{B}$ . Therefore, the influence method can be very efficient for generating many solutions using a given set of influence coefficients.

#### 5. Scaling factor technique

The influence coefficient method for cohesive crack simulations is based on the superposition of linear elastic responses, or influences, of each node on the crack face. The simulated body used to generate the influences has a specific modulus of elasticity. When used for inverse analysis, a particular test specimen geometry and size might be used with materials that have different moduli of elasticity. Generating a set of influences based on the different moduli would be computationally expensive. The scaling factor technique

<sup>2</sup> The IBM RS/6000 Scalable POWERparallel System (SP) consists of POWER2 Super Chip (P2SC) architecture RS/6000 processors, which are superscalar pipelined chips capable of executing four floating point calculations per cycle. Each processor runs at 120 MHz with 256 Mbytes of memory.

<sup>3</sup> The DEC Alpha 433au Personal Workstation uses a 21164 processor running at 433 MHz.

allows one to use a single set of influence coefficients to simulate the response of laboratory specimens with the same geometry and size but different moduli of elasticity.

5.1. How to apply the scaling factor technique

The scaling factor technique asserts that the deformation response of a simulated body with a cohesive crack and modulus of elasticity,  $E_1$  can be scaled by  $E_1/E_2$  to match the response of an identical body with a modulus  $E_2$ . This assertion leads to the requirement that the cohesive zone constitutive relationship for the simulation with modulus  $E_2$  be identical to the constitutive relationship of the body with modulus  $E_1$  except that the former is scaled along the crack opening displacement axis by the same factor,  $E_1/E_2$  (Fig. 14) [10].

As an example, consider that the solid line on the load versus displacement graph in Fig. 15 was generated from a simulated specimen with modulus of elasticity  $E_1$ . If the laboratory specimen had a modulus of elasticity of  $2E_1$  the scaling factor would be 0.5. Multiplying the displacement coordinate of

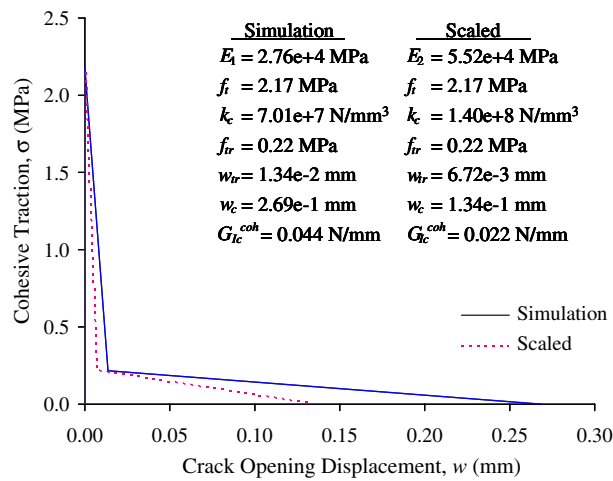


Fig. 14. Cohesive zone constitutive relationships for scaling factor example.

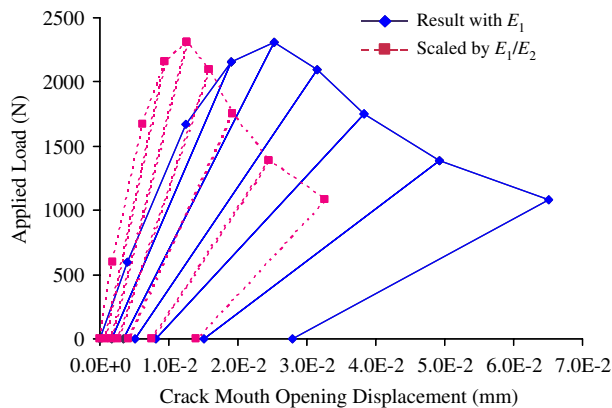


Fig. 15. Example of application of the scaling factor technique.

each point of the solid line by the scaling factor results in the graph for an identical simulated test specimen with a modulus of  $2E_1$  (the dashed line in Fig. 15). This scaled, simulated response could then be used in inverse analysis.

The cohesive zone constitutive relationship for the simulated specimen with modulus  $E_1$  is shown as the solid line in Fig. 14. Applying the scaling factor to the displacement coordinate of each point of the solid line results in the constitutive relationship for the material with a modulus of  $2E_1$  (dashed line in Fig. 14). Therefore, an identical simulated specimen with a modulus of elasticity of  $2E_1$  will generate the dashed line in Fig. 15 if the cohesive zone constitutive relationship is the dashed line in Fig. 14. If the scaled, simulated response matches the laboratory measured response, the cohesive zone property values of the laboratory specimen must be the dashed line in Fig. 14.

## 6. Conclusion

The influence coefficient method has been implemented for simulating cohesive cracking in three-dimensional bodies. An advantage of implementing the method in 3D is that the crack front is not constrained to be straight. In addition, the method has been combined with the focal point model [31] to allow simulation of unload/reload cycling of concrete. This paper has summarized the theory behind the influence coefficient method and has outlined how the method can be implemented in a numerical simulation program.

Several computational issues that affect solutions using the influence coefficient method have been identified and discussed. These issues were divided into mesh dependence and computational effort. The mesh dependence issues affect the accuracy of the solution and are reflected in the values of the influence coefficients. Verification of the accuracy of the influence coefficients will, therefore, increase the accuracy of the cohesive crack simulations. The computational issues affect the cost to generate a solution. Available memory will affect the total number of degrees of freedom that a model can have, while available time will affect the number of crack face nodes a model can have.

The scaling factor technique was developed to use a single set of influence coefficients to simulate the behavior of bodies with the same geometry but different moduli of elasticity. An example was presented.

## Acknowledgements

Development of this method has been made possible through grants by the National Science Foundation, grant # CMS-9414243, and the Alcoa Foundation, and through the use of the high-performance computing facilities at the Cornell Theory Center. The authors would like to thank Dr. Bruce Carter from the Cornell Fracture Group for his assistance with the parallel solver used to generate the flexibility coefficient matrices.

## References

- [1] Liechti KM, Wu JD. Mixed-mode, time-dependent rubber/metal debonding. *J Mech Phys Solids* 2001;49(5):1039–72.
- [2] Estevez R, Tjssens MGA, Van der Giessen E. Modeling of the competition between shear yielding and crazing of glassy polymers. *J Mech Phys Solids* 2000;48(12):2585–617.
- [3] Olbert BH. Transverse fracture of an aluminosilicate fiberboard. *J Am Ceram Soc* 1999;82(2):414–20.
- [4] Barpi F, Valente S. Numerical simulation of prenotched gravity dam models. *J Engng Mech, Am Soc Civil Engrs* 2000;126(6): 611–9.
- [5] Gopalaratnam VS, Shah SP. Softening response of plain concrete in direct tension. *J Am Concr Inst* 1985;82(3):310–23.

- [6] Hawkins NM, Yin X, Du J, Kobayashi AS. Fracture testing of CLWL-DCB specimens. In: Mihashi H, Takahashi H, Wittmann FH, editors. *Fracture toughness and fracture energy: test methods for concrete and rock*. Brookfield, VT: Balkema; 1989. p. 205–20.
- [7] Hillerborg A, Modeer M, Petersson PE. Analysis of crack formation and crack growth in concrete by means of fracture mechanics and finite elements. *Cement Concr Res* 1976;6:773–82.
- [8] Rokugo K, Iwasa M, Seko S, Koyanagi W. Tension softening diagrams of steel fiber reinforced concrete. In: Shah SP, Swartz SE, Barr B, editors. *Fracture of concrete and rock: recent developments*. Essex, England: Elsevier Applied Science; 1989. p. 513–22.
- [9] Bittencourt TN, Ingraffea AR. Three-dimensional cohesive crack analysis of short-rod specimens. In: *Fatigue and Fracture Mechanics: 25th Volume, ASTM STP 1220*. 1995. p. 46–60.
- [10] Hanson JH. An experimental–computational evaluation of the accuracy of fracture toughness tests on concrete. PhD Dissertation. Ithaca, NY: School of Civil and Environmental Engineering, Cornell University; 2000.
- [11] Kitsutaka Y. Fracture parameters by polylinear tension-softening analysis. *J Engng Mech, Am Soc Civil Engrs* 1997;123(5):444–50.
- [12] Roelfstra PE, Wittmann FH. Numerical method to link strain softening with failure of concrete. In: Wittmann FH, editor. *Fracture toughness and fracture energy of concrete*. Proceedings of the International Conference on Fracture Mechanics of Concrete, Lausanne, Switzerland. The Netherlands: Elsevier, Amsterdam; 1986. p. 163–75.
- [13] Uchida Y, Kurihara N, Rokugo K, Koyanagi W. Determination of tension softening diagrams of various kinds of concrete by means of numerical analysis. In: *Proceedings, 2nd International Conference on Fracture Mechanics of Concrete and Concrete Structures, International Association of Fracture Mechanics for Concrete and Concrete Structures (IAFraMCoS)*, Zurich, Switzerland, vol. 1, 1995. p. 17–30.
- [14] Ortiz M, Pandolfi A. Finite deformation irreversible cohesive elements for three-dimensional crack-propagation analysis. *Int J Numer Meth Engng* 1999;44(9):1267–82.
- [15] Gálvez JC, Tork B, Cendón DA, Planas J. Concrete splitting and bond in prestressed concrete beams with indented wires. In: *Proceedings, 4th International Conference on Fracture Mechanics of Concrete and Concrete Structures, International Association of Fracture Mechanics for Concrete and Concrete Structures (IAFraMCoS)*, Paris, France, vol. 1, 2001. p. 557–63.
- [16] Tvergaard V, Hutchinson JW. The relation between crack growth resistance and fracture process parameters in elastic–plastic solids. *J Mech Phys Solids* 1992;40(6):1377–98.
- [17] Dugdale DS. Yielding in steel sheets containing slits. *J Mech Phys Solids* 1960;8(2):100–4.
- [18] Barenblatt GI. In: Dryden HL, von Kármán Th, editors. *The mathematical theory of equilibrium cracks in brittle fracture*. Advances in applied mechanics, vol. 7. New York, NY: Academic Press; 1962. p. 55–129.
- [19] Petersson P-E. Crack growth and development of fracture zones in plain concrete and similar materials. Report TVBM-1006/1-174. Lund, Sweden: Division of Building Materials, Lund Institute of Technology; 1981.
- [20] Planas J, Elices M. Nonlinear fracture of cohesive materials. *Int J Fract* 1991;51(2):139–57.
- [21] Gopalaratnam VS, Ye BS. Numerical characterization of the nonlinear fracture process in concrete. *Engng Fract Mech* 1991;40(6):991–1006.
- [22] Bittencourt TN. Computer simulation of linear and nonlinear crack propagation in cementitious materials. PhD Dissertation. Ithaca, NY: Department of Civil and Environmental Engineering, Cornell University; 1993.
- [23] Bittencourt TN, Ingraffea AR. Um Método Numérico para o Modelamento de Fraturamento Coesivo em 3D. *Revista Internacional de Métodos Numéricos para Cálculo y Diseño en Ingeniería* 1995;11(4):555–64 [in Portuguese].
- [24] Bittencourt TN. Discrete approaches to cohesive-crack modeling through the finite element method. *Escola Politecnica da Universidade de Sao Paulo, Boletim Tecnico BT/PEF-9711*, 1997.
- [25] Martha LF. Topological and geometrical modeling approach to numerical discretization and arbitrary fracture simulation in three dimensions. PhD dissertation. Ithaca, NY: Department of Civil and Environmental Engineering, Cornell University; 1989.
- [26] Lutz EF. Numerical methods for hypersingular and near-singular boundary integrals in fracture mechanics. PhD dissertation. Ithaca, NY: Department of Civil and Environmental Engineering, Cornell University; 1991.
- [27] Barker LM. Residual stress effects on fracture toughness measurements. In: *Proceedings, 5th International Conference on Fracture, ICF, Cannes, France*, vol. 5, 1981. p. 2563–70.
- [28] Labuz JF, Shah SP, Dowding CH. The fracture process zone in granite: evidence and effect. *Int J Rock Mech Mining Sci Geomech Abstr* 1987;24(4):235–46.
- [29] Tosal Martínez L, Rodríguez González C, Belzunce Varela FJ, Betegón Biempica C. The influence of specimen size on the fracture behavior of a structural steel at different temperatures. *J Testing Eval, JTEVA* 2000;28(4):276–81.
- [30] Wang Y-L, Anandakumar U, Singh RN. Effect of fiber bridging stress on the fracture resistance of silicon-carbide-fiber/zircon composites. *J Am Ceram Soc* 2000;83(5):1207–14.
- [31] Yankelevsky DZ, Reinhardt HW. Uniaxial behavior of concrete in cyclic tension. *J Struct Engng, Am Soc Civil Engrs* 1989;115(1):166–82.
- [32] Press WH, Teukolsky SA, Vetterling WT, Flannery BP. *Numerical recipes in C: the art of scientific computing*. 2nd ed. Cambridge, England: Cambridge University Press; 1993. 994 pp.